Saudi Pharmaceutical Journal 31 (2023) 101735

HOSTED BY

Contents lists available at ScienceDirect

Saudi Pharmaceutical Journal

journal homepage: www.sciencedirect.com

Original article

One-step preparation, characterization, and anticancer potential of $ZnFe_2O_4$/RGO nanocomposites

ZabnAllah M. Alaizeri *, Hisham A. Alhadlaq, Saad Aldawood, Mohd Javed Akhtar, Maqusood Ahamed *

Department of Physics and Astronomy, College of Science, King Saud University, Riyadh 11451, Saudi Arabia

ARTICLE INFO

Article history:
Received 14 May 2023
Accepted 30 July 2023
Available online 5 August 2023

Keywords:
$ZnFe_2O_4$/RGO
Facile synthesis
Band gap tuning
Physicochemical properties
Anticancer activity

ABSTRACT

Zinc ferrite nanoparticles ($ZnFe_2O_4$ NPs) have attracted extensive attention for their diverse applications including sensing, waste-water treatment, and biomedicine. The novelty of the present work is the fabrication of $ZnFe_2O_4$/RGO NCs by using a one-step hydrothermal process to assess the influence of RGO doping on the physicochemical properties and anticancer efficacy of $ZnFe_2O_4$ NPs. X-ray diffraction (XRD), Scanning electron microscopy (SEM), Energy-dispersive X-ray(EDX), X-ray photoelectron spectroscopy (XPS), Fourier-transform infrared spectroscopy (FTIR), UV–vis spectroscopy, and Photoluminescence (PL) spectroscopy were employed to characterize prepared pure $ZnFe_2O_4$ NPs and $ZnFe_2O_4$/ RGO NCs. XRD results showed that the synthesized samples have high crystallinity. Furthermore, the average crystal sizes of $ZnFe_2O_4$ nanoparticles (NPs) and $ZnFe_2O_4$/RGO nanocomposites (NCs) were 51.08 nm and 54.36 nm, respectively. SEM images revealed that pure $ZnFe_2O_4$ NPs were spherical in shape with uniformly loaded on the surface of the RGO nanosheet. XPS and EDX analysis confirmed the elemental compositions of $ZnFe_2O_4$/RGO NCs. Elemental mapping of SEM shows that the elemental compositions (Zn, Fe, O, and C) were homogeneously distributed in $ZnFe_2O_4$/RGO NCs. The intensity of FT-IR spectra depicted that pure $ZnFe_2O_4$ NPs were successfully anchored into the RGO nanosheet. An optical study suggested that the band gap energy of $ZnFe_2O_4$/RGO NCs (1.61 eV) was lower than that of pure $ZnFe_2O_4$ NPs (1.96 eV). PL spectra indicated that the recombination rate of the $ZnFe_2O_4$/ RGO NCs was lower than $ZnFe_2O_4$ NPs. MTT assay was used to evaluate the anticancer performance of $ZnFe_2O_4$ /RGO NCs and pure $ZnFe_2O_4$NPs against human cancer cells. In vitro study indicates that $ZnFe_2O_4$ /RGO NCs have higher anticancer activity against human breast (MCF-7) and lung (A549) cancer cells as compared to pure form $ZnFe_2O_4$ NPs. This work suggests that RGO doping enhances the anticancer activity of $ZnFe_2O_4$NPs by tuning its optical behavior. This study warrants future research on potential therapeutic applications of these types of nanocomposites.

© 2023 The Author(s). Published by Elsevier B.V. on behalf of King Saud University. This is an open access article under the CC BY-NC-ND license (http://creativecommons.org/licenses/by-nc-nd/4.0/).

1. Introduction

Cancer remains one of the most significant health challenges worldwide, necessitating the continuous exploration of novel therapeutic strategies. However, it is recently a complex and deadly disease that affects millions of people worldwide (Bray et al., 2018). Despite progress in cancer treatment, there is an urgent requirement for the creation of new therapeutic approaches that are both efficient and safe (Shyamala and Gomathi Devi, 2020; Tabrez et al., 2022a; Zughaibi et al., 2022). One promising approach is applied of nanocomposites(NCs) which have shown great potential in enhancing anticancer performance (Ahamed et al., 2023a; Saranya et al., 2023). Nowadays, some challenges of cancer treatment are the synthesis and characterization of nanocomposites with optimal physicochemical properties (Biswal and Yusoff, 2017).

To solve these challenges, previous studies have focused on the synthesis of nanocomposites (NCs) using a variety of methods (Kokila et al., 2022; Saranya et al., 2023; Somwanshi et al., 2020). Among the various types of NCs, metal oxide /reduced graphene oxide (RGO) nanocomposites (NCs) are being applied in potential applications owing to their outstanding properties such as high surface area and good biocompatibility (Aarti et al., 2022). For example, $ZnFe_2O_4$ NPs have been combined with reduced graphene

* Corresponding authors.
E-mail addresses: zalaizeri@ksu.edu.sa (ZabnAllah M. Alaizeri), mahamed@ksu.edu.sa (M. Ahamed).

Peer review under responsibility of King Saud University.

Production and hosting by Elsevier

https://doi.org/10.1016/j.jsps.2023.101735
1319-0164/© 2023 The Author(s). Published by Elsevier B.V. on behalf of King Saud University.
This is an open access article under the CC BY-NC-ND license (http://creativecommons.org/licenses/by-nc-nd/4.0/).

oxide (RGO) as NCs to enhance the properties of $ZnFe_2O_4$ NPs, which can be performed in potential applications (Khadgi et al., 2016; Wu et al., 2015). However, the nanocomposites (NCs) have been prepared using several approaches including, Physical Vapor Deposition (PVD)(Nguyen et al., 2019), Chemical Vapor Deposition (CVD) (Nguyen et al., 2019), green approach (Prasad et al., 2017), sol–gel method (Banerjee et al., 2018), and hydrothermal/-solvothermal method (Khadgi et al., 2016). In another instance, (Ahamed et al. (Ahamed et al., 2022) synthesized ZnO/RGO NCs by a green approach. This study revealed that prepared ZnO/RGO NCs have been shown to enhance the therapeutic efficacy of doxorubicin in breast cancer cells.

Interestingly, zinc ferrite ($ZnFe_2O_4$) NPs have been extensively studied in potential biomedical applications due to their unique physiochemical properties (Aarti et al., 2022). Krishnan et al (Krishnan et al., 2021) prepared $ZnFe_2O_4$/RGO NCs via a facile green approach. This study showed that the $ZnFe_2O_4$/RGO NCs have a high cytotoxicity effect against human lung cancer(A549) cells. In another study, Au/RGO NCs exhibited high cytotoxicity against human colon cancer cell lines (HT-29 and SW-948), while it has high cytocompatibility toward normal human colon (CCD-841) (Al-Ani et al., 2019). Similarly, TiO_2/ RGO NCs have been applied as fluorescent probes for the imaging and detection of cancer cells (Umekar et al., 2021). Lee et al (Lee et al., 2015) showed that the Fe_3O_4/ RGO NCs exhibit as contrast agents for magnetic resonance imaging (MRI).

The present study aimed to investigate the novel application of RGO to improve the physicochemical properties of $ZnFe_2O_4$ NPs and their potential in anticancer therapy. Pure $ZnFe_2O_4$ NPs and $ZnFe_2O_4$/RGO NCs were successfully prepared by using One-step hydrothermal synthesis. X-ray diffraction (XRD), scanning electron microscopy (SEM), energy-dispersive X-ray (EDX), X-ray photoelectron (XPS), Furrier Infrared (FTIR), UV–vis spectroscopy, and photoluminescence (PL)spectrometer were applied to characterize the physicochemical properties. Cytotoxicity study showed that the $ZnFe_2O_4$/RGO NCs induced high cytotoxicity against MCF-7 and A549 cancer cells compared with pure $ZnFe_2O_4$ NPs.

2. Experimental part

2.1. Chemicals

Iron (III) nitrate nonahydrate ($Fe(NO_3)_3{\cdot}9H_2O$), Zinc nitrate hexahydrate ($Zn(NO_3)_2{\cdot}6H_2O$), Graphene oxide (GO), Sodium hydroxide (NaOH), and Ethylene glycol (EG) were supplied from Sigma Aldrich. The preparation was carried out using distilled water (DW) as the medium. These chemicals were used as received without undergoing any additional purification.

2.2. Synthesis of pure $ZnFe_2O_4$ NPs and $ZnFe_2O_4$/RGO NCs

Pure $ZnFe_2O_4$ NPs and $ZnFe_2O_4$/RGO NCs were successfully prepared by one-step hydrothermal approach (Behera et al., 2019). The 1 g of $Fe(NO_3)_3{\bullet}9H_2O$ and 0.5 g of $Zn(NO_3)_2{\bullet}6H_2O$ were dissolved in 50 ml of EG under continuous stirring for 1 h. Then, the 800 mg of GO was also dispersed in DI water and added to the above solution under sonication for 30 min. Next, 10 ml of NaOH (2 M) was gradually added drop into the mixture to reach PH = 12. The mixture solution was stirred for 1 h and further transferred into a Teflon-lined autoclave, and heated at 140 °C for 12 h. After that, the precipitate was collected by centrifugation and washed several times with DI water and ethanol. Finally, this precipitate was dried in the oven at 80 °C for 12 h. The dried precipitate was crushed into powder using a mortar and pestle. Pure $ZnFe_2O_4$ NPs were synthesized using the same above procedures without GO. A similar procedure was further used for the preparation of RGO without mixing ($Fe(NO_3)_3{*}9H_2O$, $Zn(NO_3)_2{*}6H_2O$). The synthesis protocol of $ZnFe_2O_4$/RGO NCs was depicted in Scheme 1.

2.3. Characterization

Different analytical techniques were employed to characterize the prepared $ZnFe_2O_4$ NPs and $ZnFe_2O_4$/RGO NCs. X-ray diffraction (XRD) (PanAnalytic X'Pert Pro, Malvern Instruments, Malvern, UK) was used to examine their crystal structure and phase purity. Morphological analysis of prepared samples was carried out using scanning electron microscopy (SEM) (SEM, JSM-7600F, JEOL, Inc. Tokyo, Japan). Energy-dispersive X-ray spectroscopy (EDX) and X-ray photoelectron spectroscopy (XPS) (PHI-5300 ESCA PerkinElmer, Boston, MA, USA)were utilized to determine the chemical composition and oxidation states of the prepared samples. Fourier transform infrared spectroscopy (FTIR) was used to study their functional groups. To investigate their optical properties, UV–Vis (Hitachi U-2600) and photoluminescence (PL) Hitachi F-4600) spectroscopy were employed to determine the band gap energy of the NPs and NCs.

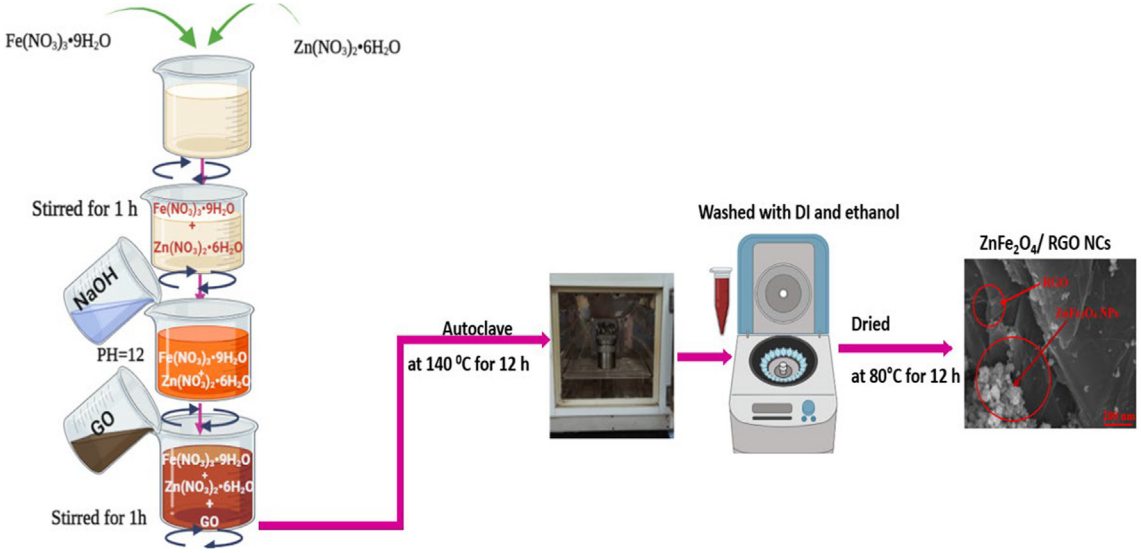

Scheme 1. Synthesis protocol of $ZnFe_2O_4$/RGO NCs.

2.4. Cell culture

Human breast cancer (MCF-7) and human lung cancer (A549) cells were supplied from America (ATTC, Manassas, WV, USA). These cell lines were cultured in Dulbecco's Modified Eagle's Medium (DMEM) with high glucose, along with 10% fetal bovine serum (FBS), 1% L-glutamine, and 1% penicillin–streptomycin supplementation. The cells were then incubated in a humidified environment at 37 °C with 5% CO_2.

2.5. Cytotoxicity assay

The MTT assay was utilized to assess the cytotoxicity of the prepared samples. To further implement the MTT assay on pure $ZnFe_2O_4$ NPs and $ZnFe_2O_4$/rGO NCs, the following procedures were carried out. Initially, MCF-7 and A549 cells were seeded at a density of $1x10^4$ cells per well in 96-well plates and then incubated at 37 °C with 5% CO2 for 24 h. Following that, the cells were exposed to various concentrations (ranging from 1.5 µg/ml to 200 µg/ml) of the synthesized samples in an incubator at 37 °C with 5% CO2 for 24 h. Subsequently, 100 µL of MTT solution was added to each well and then incubated for 3 h. Finally, 100 µL of DMSO was added to dissolve the formazan crystals in each well. The absorbance of the final solution was measured at 570 nm utilizing a microplate reader.

2.6. Statistical analysis

The analysis of biological data was carried out using one-way ANOVA and Dunnett's multiple comparison test. Statistical significance was further $p < 0.05$.

3. Results

3.1. XRD study

Fig. 1 depicts the XRD spectra of RGO, $ZnFe_2O_4$ NPs, and $ZnFe_2O_4$/RGO NCs. XRD spectra of RGO (Fig. 1a) showed that the RGO has a high peak at 26° and 43.02° which corresponds to (002) and (102) planes. It can be seen in Fig. 1b that the diffraction peaks of the $ZnFe_2O_4$ NPs at 2θ values of 17.29.70°, 35°, 42.64°, 52.90°, 56.50°, 62.12°, and 73.40° correspond to the (220), (311), (400), (422), (511), (440), and (533) planes of the spinel structure of $ZnFe_2O_4$ (JCPDS card no. 01–79-1905). Fig. 1c showed that the diffraction peaks were assigned at 2θ values of 30.02°, 35.48°, 43.24°, 53.64°, 57.00°, 62.72°, and 74.00° correspond to the (220), (311), (400), (422), (511), (440), and (533) crystal planes respectively. Furthemore, it was observed that the average crystal sizes of $ZnFe_2O_4$ NPsand $ZnFe_2O_4$/RGO NCs were 51.08 nm and 54.36 nm, respectively, which were calculated by the Scherrer equation.

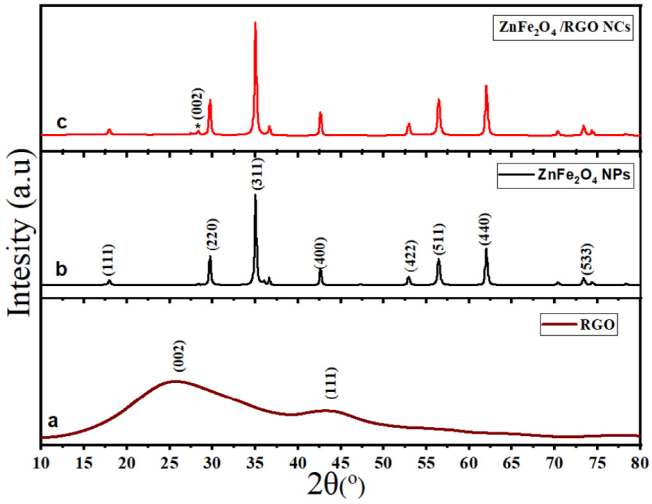

Fig. 1. XRD spectra of RGO (a), $ZnFe_2O_4$ NPs (b), and $ZnFe_2O_4$/RGO NCs (c).

3.2. SEM analysis

SEM and EDX analysis of the synthesized samples provide valuable information about their morphology, structure, and elemental composition. The SEM images and EDX data of pure $ZnFe_2O_4$ NPs and $ZnFe_2O_4$/RGO NCs were illustrated in Fig. 2. However, the SEM image of $ZnFe_2O_4$ NPs displayed uniform distributions of spherical particles with agglomerations. The EDX spectra (Fig. 2b) of $ZnFe_2O_4$ NPs confirmed the presence of zinc (Zn), iron (Fe), and oxygen (O) elements. Moreover, SEM images of $ZnFe_2O_4$/RGO NCs(Fig. 2c)showed that the presence of $ZnFe_2O_4$ NPs was successfully anchored onto the RGO nanosheet. $ZnFe_2O_4$/RGO NCs were prepared by integrating $ZnFe_2O_4$ NPs onto the RGO nanosheet. Furthermore, the elemental composition (Zn, Fe, O, and C) of both $ZnFe_2O_4$ NPs and RGO were further confirmed in EDX spectra (Fig. 2d). Fig. 3b-e demonstrated the SEM elemental mapping of $ZnFe_2O_4$/RGO NCs, which confirmed the uniform distribution of all elements (Zn, Fe, O, and C) in the synthesized samples.

3.3. XPS study

Fig. 4 shows the full scan of XPS spectra of $ZnFe_2O_4$/RGO NCs, with high-resolution spectra of Zn 2p, Fe 2p, O1s, and C1s. The binding energy (B.E) of Zn in the $ZnFe_2O_4$/RGO NCs was shown in the high-resolution XPS spectra of Zn 2P (Fig. 4 b). As shown in Fig. 4b, the Zn 2P peaks were observed at 1021.68 eV and 1045 eV for Zn $2P_{3/2}$ and Zn $2P_{3/2}$, respectively(Lai et al., 2021). In Fig. 4 c, the high-resolution XPS spectra of Fe 2P display peaks at 711.31 eV and 725.32 eV for the tetrahedral Fe $2p_{3/2}$ and octahedral Fe $2p_{1/2}$, respectively. The peaks of C 1 s (Fig. 4d) were detected at 288.01 eV, 286.43 eV, 284.84 eV, and 283.57 eV, which corresponded to the C = O bond, C-O bond (epoxy and hydroxyl), C–C bond, and C = C bond, respectively. Similarly, Fig. 4e displays the high-resolution XPS spectra of O 1 s, which reveals a peak at 529.3 due to the interaction between Fe-O of the $ZnFe_2O_4$/RGO NCs. In addition, the peak located at 531.1 eV indicates the presence of O-C-O bonding, while the peak at 532.2 eV indicates the presence of Fe-C-O bonding.

3.4. FTIR study

The functional group of $ZnFe_2O_4$ NPs and $ZnFe_2O_4$/ RGO NCs are shown in FT-IR spectra(Fig. 5). It can be seen in Fig that the $ZnFe_2O_4$ NPs exhibit absorption peaks at 558.82 and 402.10 cm^{-1}, which were assigned to Zn–O and Fe–O bonds, respectively. These peaks could be attributed to different vibrational modes of the metal oxide NPs. The C = O and C = C stretching vibrations were associated at 1964.31 and 2138 cm^{-1} for $ZnFe_2O_4$ NPs and $ZnFe_2O_4$/ RGO NCs, respectively. Additionally, the RGO shows characteristic peaks at around 1613.90 cm^{-1} that can be attributed to C = C stretching vibrations. Moreover, the absorption bands of $ZnFe_2O_4$ NPs and $ZnFe_2O_4$/ RGO NCs at around 3551.11 cm^{-1} correspond to the stretching vibration of O–H groups.

3.5. UV analysis

UV spectroscopy is a commonly employed analytical technique to study the optical properties of synthesized samples. As shown in

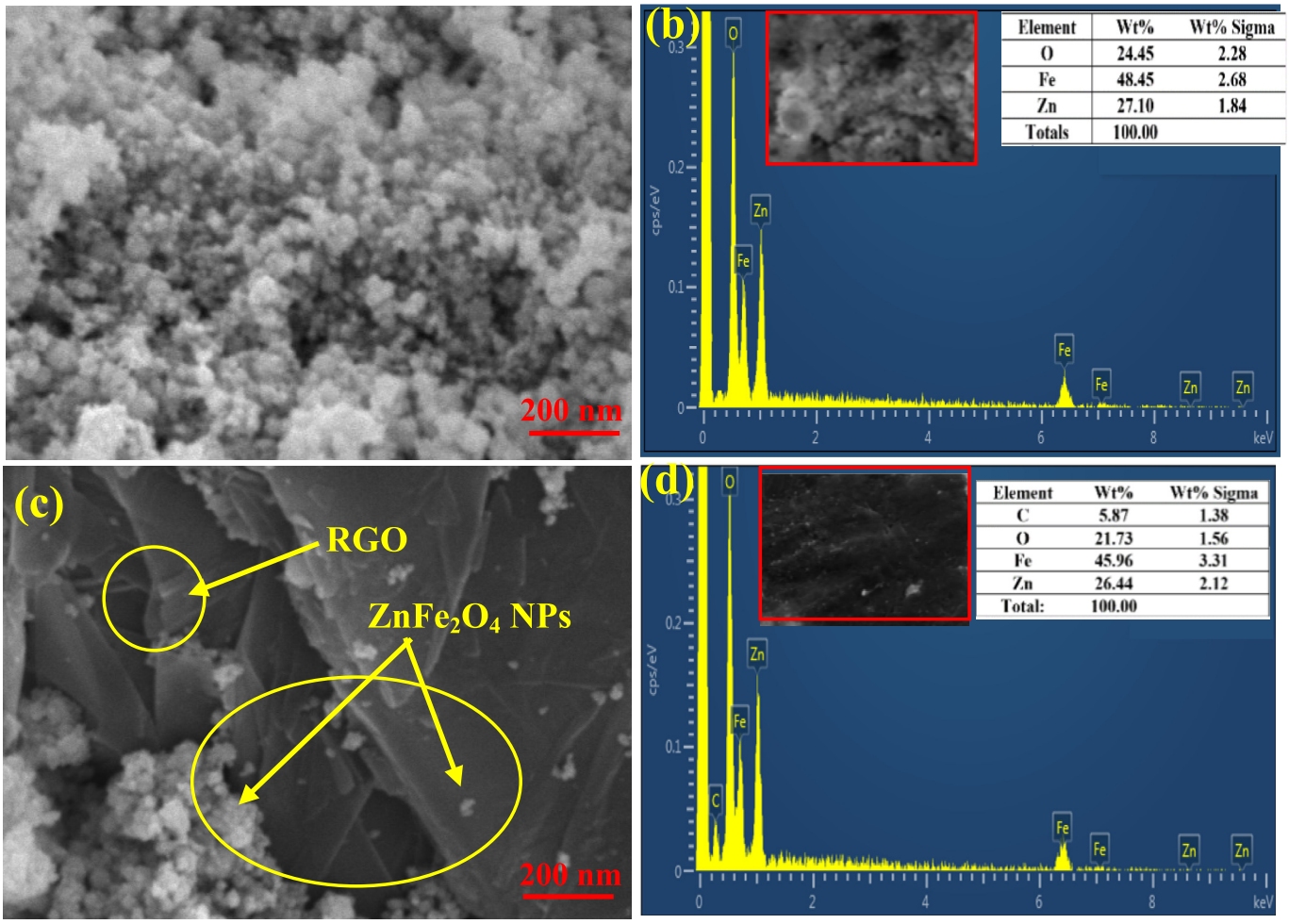

Fig. 2. (a) Image SEM of $ZnFe_2O_4$ NPs, (b)EDX of $ZnFe_2O_4$ NPs, (c) Image SEM of $ZnFe_2O_4$/ RGO NCs, (b)EDX of $ZnFe_2O_4$/ RGO NCs.

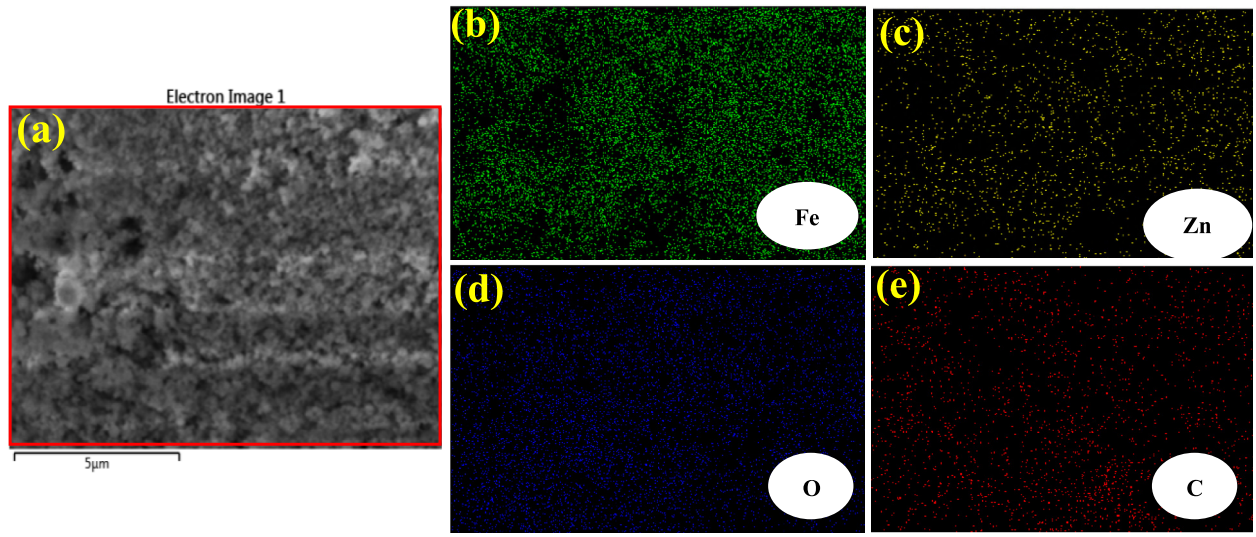

Fig. 3. Elemental mapping of $ZnFe_2O_4$/RGO NCs, SEM image (a), Iron (Fe) (b), zinc (Zn)(c), oxygen(O) (d), and carbon (C)(e).

Fig. 6, the UV–Vis spectra of $ZnFe_2O_4$ NPs and $ZnFe_2O_4$/ RGO NCs were investigated. In particular, the UV spectra (Fig. 6a) displayed absorption peaks at 632.65 nm and 770.18 nm for $ZnFe_2O_4$ NPs and $ZnFe_2O_4$/RGO NCs, respectively. This process indicates that the band gap energy of the $ZnFe_2O_4$/RGO NCs decreased with RGO doping. The band gap energy (Eg) of synthesized samples was calcu-

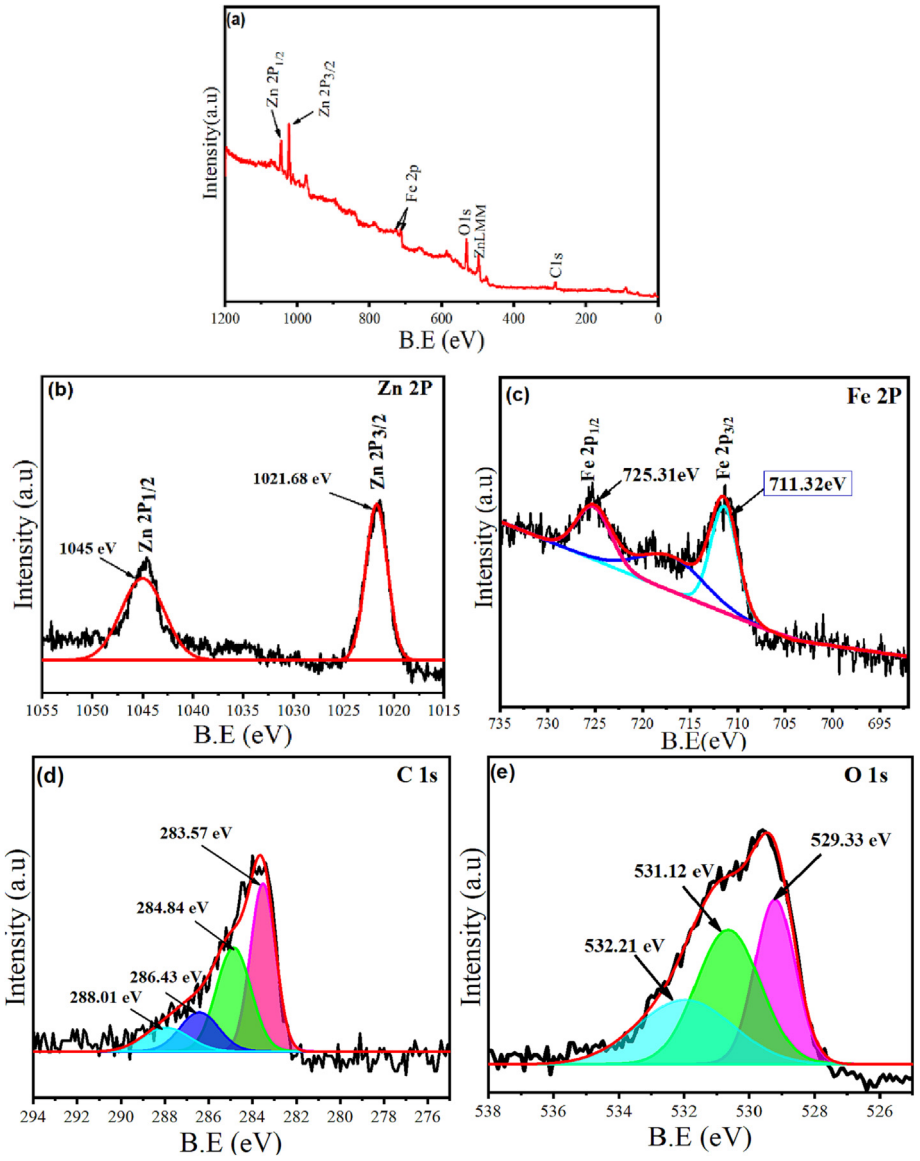

Fig. 4. (a) The full scan of XPS spectra of $ZnFe_2O_4$/RGO NCs, (b) high resolution of XPS of Zn 2P, (c) high resolution of XPS of Fe 2P, (d) high resolution of XPS of O 1 s and (e) high resolution of XPS of C 1 s in $ZnFe_2O_4$/RGO NCs.

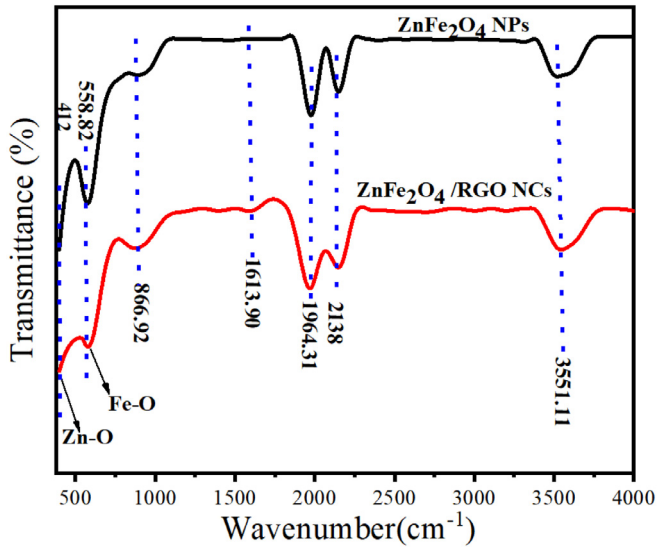

Fig. 5. FT-IR spectra of $ZnFe_2O_4$ NPs and $ZnFe_2O_4$/ RGO NCs.

lated by Tauc plot analysis (Fig. 6b). Furthermore, $ZnFe_2O_4$ NPs and $ZnFe_2O_4$/RGO NCs have band gap energies (Eg) of 1.96 and 1.61 eV, respectively.

3.6. PL analysis

The migration rate of electrons and holes in $ZnFe_2O_4$ NPs and $ZnFe_2O_4$/ RGO NCs was measured using photoluminescence (PL). Fig. 7 illustrates the PL spectra of the synthesized samples at room temperature using an excitation wavelength of 355 nm. The addition of dopant to RGO led to a decrease in the emission peak observed at 481 nm. As shown in Fig. 7, the PL intensity of $ZnFe_2O_4$ NPs was slightly reduced in the presence of RGO sheet. This reduction in PL intensity can be attributed to the improved charge transfer that occurs between RGO and $ZnFe_2O_4$ NPs. Consequently, the strong electrical conductivity of RGO sheets facilitates effective separation of electron-hole (e-/h +) pairs. PL spectra indicated that the recombination rate of the $ZnFe_2O_4$/ RGO NCs was lower than $ZnFe_2O_4$ NPs due to the interaction between $ZnFe_2O_4$ and RGO.

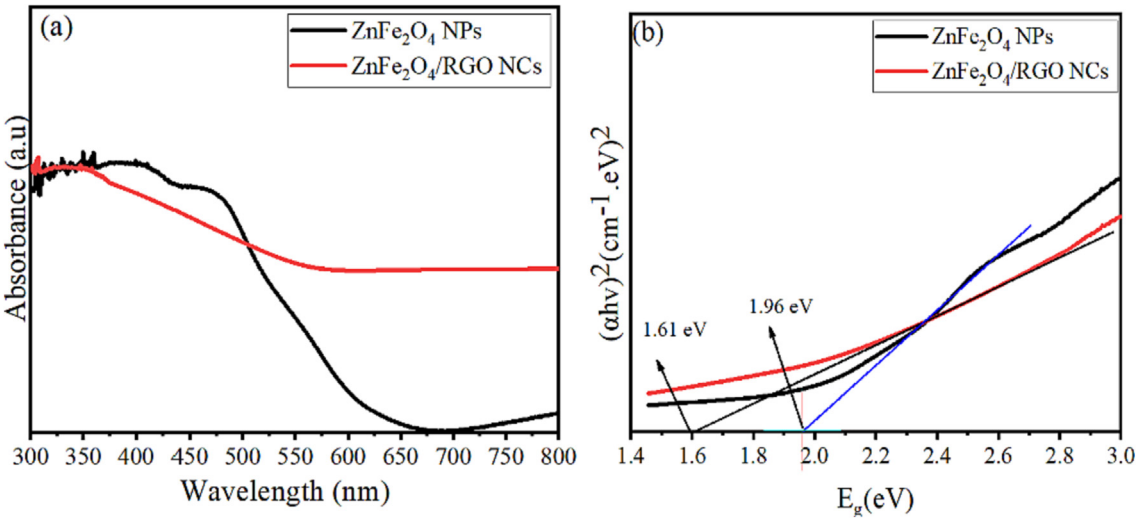

Fig. 6. (a)UV spectra of $ZnFe_2O_4$ NPs and $ZnFe_2O_4$/ RGO NCs, and (b) the band gap energy (E_g) of $ZnFe_2O_4$ NPs and $ZnFe_2O_4$/ RGO NCs.

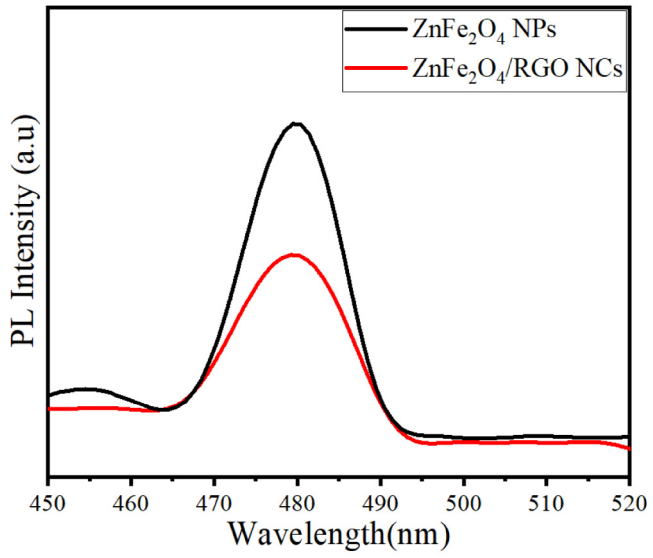

Fig. 7. PL spectra of $ZnFe_2O_4$ NPs and $ZnFe_2O_4$/ RGO NCs.

3.7. Cytotoxicity performance

The cytotoxicity effect of pure $ZnFe_2O_4$NPs and $ZnFe_2O_4$/RGO NCs by using the MTT assay toward two cancer cells ((MCF-7 and A549) was presented in Fig. 8a and b. We observed (Fig. 8a) that the cell viability of MCF-7 cells decreased with increasing concentrations of pure $ZnFe_2O_4$NPs and $ZnFe_2O_4$/RGO NCs. Similarly, the cell viability of the A549 cells (Fig. 8b) reduced with an increase in the concentrations (1.5–200 μg/mL) of the synthesized samples. Fig. 8a and b showed the cytotoxicity performance of $ZnFe_2O_4$/RGO NCs toward the MCF-7 and A549 was greater than pure $ZnFe_2O_4$ NPs. The IC50 values of $ZnFe_2O_4$ NPs and $ZnFe_2O_4$/RGO NCs toward two types of human cancer cells were presented in Table 1.

The graphene-based nanocomposites have demonstrated promising anticancer activity against human cancer cells in vitro studies through several mechanisms. In the present study, the prepared nanocomposites can interact with cellular membranes and intracellular organelles, disrupting vital cellular processes in cancer cells. Furthermore, these synthesized nanocomposites are ṡuptake by cancer cells through receptor-mediated endocytosis to produce reactive oxygen species (ROS). These ROS are oxygen radicals capable of death cancer cells by causing oxidative damage to killing cells. For example, synthesized ZrO_2-ZnO/RGO NCs have been found to induce oxidative stress in cancer cells, leading to DNA damage (Ahamed et al., 2023b).

4. Discussion

In the present work, the $ZnFe_2O_4$/RGO NCs were synthesized using a simple one-step hydrothermal method and characterized using various techniques such as XRD, SEM, EDX, XPS, FTIR, UV–vis spectroscopy, and PL spectrometer. XRD data indicate that the $ZnFe_2O_4$/RGO NCs exhibited high purity and good crystallinity, with the $ZnFe_2O_4$ NPs uniformly distributed on the RGO surface. (Hidayah et al., 2017). Furthermore, average crystal sizes were increased with RGO doping, which was calculated by the Scherrer equation (Patterson, 1939). XRD results show the successful synthesis of the $ZnFe_2O_4$/RGO NCs, which agrees with previous studies (Kaur et al., 2018; Wang and Shih, 2021). As shown in the SEM image, $ZnFe_2O_4$ NPs displayed uniform distributions of spherical particles with agglomerations (Sripriya et al., 2018). EDX analysis confirmed that the elemental composition of both $ZnFe_2O_4$ NPs and RGO were Zn, Fe, O, and C elements. Moreover, the uniform distribution of all elements (Zn, Fe, O, and C) in the synthesized $ZnFe_2O_4$/RGO NCs was investigated by SEM elemental mapping. The elemental composition and chemical state of the prepared samples were determined by the XPS technique. Importantly, the peaks at 531.1 eV and 532.2 eV represent O-C-O and Fe-C-O bonding, respectively, which were in good agreement with earlier studies (Hou et al., 2015; Shah et al., 2013; Yuan et al., 2015; Zhang et al., 2016; Zhao et al., 2017). These results were supported by EDX data.

The functional groups of prepared samples were further carried out by FTIR spectroscopy. In $ZnFe_2O_4$/ RGO NCs, new peaks were observed at approximately 1613.90 cm^{-1}, which are indicative of the stretching vibrations of C = C bonds in RGO. This peak was not appeared in the FTIR spectra of $ZnFe_2O_4$NPs, indicating the absence of RGO as shown in this study(Sarala et al., 2020). This phenomenon indicated that $ZnFe_2O_4$NPs were successfully anchored on the RGO sheet. FTIR spectra revealed that the intensities of the absorption bands of $ZnFe_2O_4$/ RGO NCs reduced due to the presence of the RGO sheet (Zamani et al., 2020). FTIR results

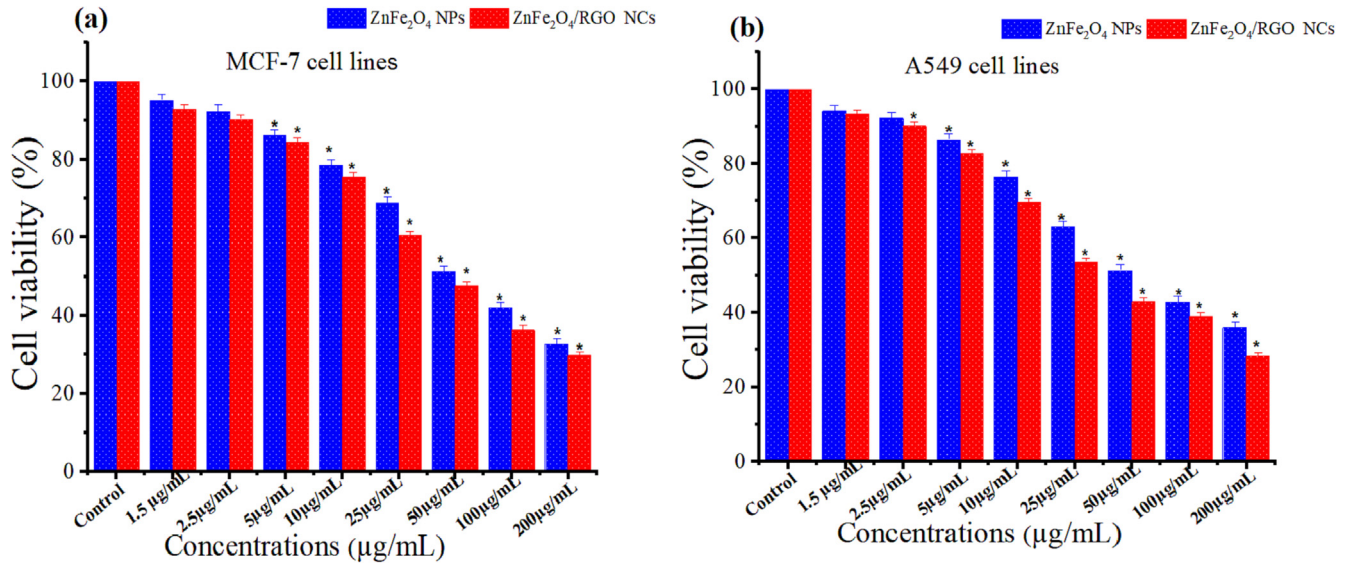

Fig. 8. (a) Cell viability of MCF-7 cells with different concentrations of $ZnFe_2O_4$ NPs and $ZnFe_2O_4$/RGO NCs for 24 h and (b) Cell viability of A549 cells with different concentrations of $ZnFe_2O_4$ NPs and $ZnFe_2O_4$/RGO NCs for 24 h by using the MTT assay. * Significantly different from control ($p < 0.05$).

Table 1
The IC_{50} values (µg/mL) of synthesized samples for two types of human cancer cells.

Cell lines	$ZnFe_2O_4$ NPs	$ZnFe_2O_4$/RGO NCs
MCF-7	64.25	48.28
A549	65.51	46.70

were excellent and in agreement with XRD results and previous investigators (Li and Zhou, 2020; Riaz et al., 2022).

The optical properties of synthesized samples were performed by UV–vis spectroscopy. Interestingly, the UV spectra of $ZnFe_2O_4$/RGO NCs exhibited a shift in the position of the peaks compared to pure $ZnFe_2O_4$ NPs due to the interaction between $ZnFe_2O_4$ NPs and RGO as supported in these studies (Nadeem et al., 2020; Xie et al., 2013). Furthermore, the band gap energy (Eg) of $ZnFe_2O_4$ NPs and $ZnFe_2O_4$/ RGO NCs were 1.96 eV and 1.61 eV, respectively, which were according with earlier research (Wu et al., 2015). The recombination rate of $ZnFe_2O_4$ NPs and $ZnFe_2O_4$/ RGO NCs was further evaluated using a photoluminescence (PL) spectrometer. PL results showed that the reduction of the emission peak at 481 nm of $ZnFe_2O_4$ NPs was observed with RGO doping. The PL intensity of the $ZnFe_2O_4$ NPs was lower than that of $ZnFe_2O_4$ 4/ RGO NCs. The reduction of PL intensity could be attributed to the enhanced charge transfer between the RGO and $ZnFe_2O_4$ NPs (Khadgi et al., 2017). Additionally, the RGO sheets have strong electrical conductivity as the electron source to effectively separate the electron-hole (e^-/h^+) pair (Hou et al., 2013). These results suggested that $ZnFe_2O_4$/ RGO NCs can be applied in potential applications including, photocatalytic and cancer treatment (Behera et al., 2018; Renukadevi and Pricilla Jeyakumari, 2020).

Due to their unique properties, many researchers have been interested in applying metal oxide NPs and graphene-based NCs in biomedicine and cancer therapy (Alafaleq et al., 2023; Alaizeri et al., 2022; Arunima Rajan et al., 2019; Krishnan et al., 2021; Sarala et al., 2020; Tabrez et al., 2022c, 2022b). In this work, the MTT experiment was carried out on two different cancer cell lines (MCF-7 and A549) to assess the anticancer activity of synthesized samples. It was observed that $ZnFe_2O_4$/RGO NCs exhibited higher cytotoxicity towards the cancer cell lines (MCF-7 and A549) compared to pure $ZnFe_2O_4$ NPs exhibiting IC50 around 50 for 24 h. At the same interval time, previous studies have observed significant cytotoxicity of metal with RGO in various cancer cell types, including HepG2, and A549 cells, with IC_{50} concentrations of approximately 100 µg/mL and 250 µg/mL (Alaizeri and Alhadlaq, 2022; Krishnan et al., 2021). Our results suggest that RGO doping in $ZnFe_2O_4$ NPs enhances their anticancer performance against human cancer (MCF-7 and A549) cells.

5. Conclusion

In the present work, one-step hydrothermal synthesis was successfully used to prepare the $ZnFe_2O_4$ NPs and $ZnFe_2O_4$/RGO NCs. Physicochemical properties of pure $ZnFe_2O_4$ NPs and $ZnFe_2O_4$/ RGO NCs were further investigated by different analytical techniques such as XRD, SEM, XPS, UV–Vis, FTIR, and PL. XRD results showed that the prepared samples have high crystallinity. Furthermore, the average crystal sizes of $ZnFe_2O_4$ NPs increased with the addition of the RGO sheet. SEM images demonstrate that $ZnFe_2O_4$ NPs were successfully anchored on the RGO nanosheets. The elemental compositions of $ZnFe_2O_4$/RGO NCs were confirmed by XPS and EDX analysis. SEM elemental mapping revealed a uniform distribution of zinc (Zn), iron (Fe), oxygen (O), and carbon (C) within the $ZnFe_2O_4$/RGO NCs. FT-IR spectra confirmed that the functional group of prepared samples was changed with RGO adding. UV–vis spectra showed the absorption peak of $ZnFe_2O_4$ NPs affected by RGO doping. This process indicates that the band gap energy of $ZnFe_2O_4$/RGO NCs (1.96 eV) is lower than pure $ZnFe_2O_4$ NPs (1.61 eV). PL results showed that the $ZnFe_2O_4$/ RGO NCs have a lower recombination rate than $ZnFe_2O_4$ NPs**.** Biological results showed that the $ZnFe_2O_4$ /RGO NCs exhibit higher anticancer activity in human cancer cells (MCF-7 and A549) than pure $ZnFe_2O_4$ NPs. This study suggests that RGO plays a crucial role in improving the anticancer potential of $ZnFe_2O_4$ NPs by tuning its optical properties. The results of this study warrant further inquiry into the potential therapeutic applications of nanocomposites created by $ZnFe_2O_4$ NPs and RGO sheets. In this work, the one-step preparation, characterization, and anticancer potential of $ZnFe_2O_4$/RGO NCs provides valuable insights into the field of nanomaterials for cancer therapy. However, certain limitations and areas for future research should be acknowledged. One of the limitations of this study is synthesis parameters, such as reaction time, temperature,

and precursor concentrations, which affect improved control over the nanocomposite morphology and properties. Additionally, further in vitro and in vivo studies are required to comprehensively evaluate their therapeutic efficacy and safety profiles.

Declaration of Competing Interest

The authors declare that they have no known competing financial interests or personal relationships that could have appeared to influence the work reported in this paper.

Acknowledgment

The authors extend their sincere appreciation to researchers supporting project number (RSPD2023R813), King Saud University, Riyadh, Saudi Arabia for funding this research.

References

Aarti, Gaur, A., Chand, P., Shah, J., Kotnala, R.K., 2022. Tin Oxide (SnO2)-Decorated Reduced Graphene Oxide (rGO)-Based Hydroelectric Cells to Generate Large Current. ACS Omega 7, 43647–43656. https://doi.org/10.1021/acsomega.2c04553

Ahamed, M., Lateef, R., Khan, M.A.M., Rajanahalli, P., Akhtar, M.J., 2023b. Biosynthesis, Characterization, and Augmented Anticancer Activity of ZrO2 Doped ZnO/rGO Nanocomposite. J. Funct. Biomater. 14. https://doi.org/10.3390/jfb14010038

Ahamed, M., Javed Akhtar, M., Majeed Khan, M.A., Alhadlaq, H.A., 2022. Facile green synthesis of ZnO-RGO nanocomposites with enhanced anticancer efficacy. Methods 199, 28–36. https://doi.org/10.1016/j.ymeth.2021.04.020.

Ahamed, M., Akhtar, M.J., Khan, M.A.M., 2023a. ZrO_2 nanoparticles anchored on RGO sheets: Eco-friendly synthesis from Acacia nilotica (L.) fruit extract, characterization, and enhanced anticancer activity in different human cancer cells. Materialstoday Communications 36, 106756. https://doi.org/10.1016/j.mtcomm.2023.106756.

Alafaleq, N.O., Zughaibi, T.A., Jabir, N.R., Khan, A.U., Khan, M.S., Tabrez, S., 2023. Biogenic synthesis of Cu-Mn bimetallic nanoparticles using pumpkin seeds extract and their characterization and anticancer efficacy. Nanomaterials 13, 1–13. https://doi.org/10.3390/nano13071201.

Alaizeri, Z.M., Alhadlaq, H.A., 2022. One-Pot Synthesis of SnO 2 -rGO Nanocomposite for Enhanced Photocatalytic and Anticancer Activity.

Alaizeri, Z.M., Alhadlaq, H.A., Aldawood, S., Akhtar, J., Ahamed, M., 2022. One-Pot Synthesis of SnO 2-rGO Nanocomposite for Enhanced Photocatalytic and Anticancer Activity. https://doi.org/10.3390/polym14102036.

Al-Ani, L.A., Yehye, W.A., Kadir, F.A., Hashim, N.M., AlSaadi, M.A., Julkapli, N.M., Hsiao, V.K.S., 2019. Hybrid nanocomposite curcumin-capped gold nanoparticle-reduced graphene oxide: Antioxidant potency and selective cancer cytotoxicity. PLoS One 14, 1–24. https://doi.org/10.1371/journal.pone.0216725.

Arunima Rajan, S., Khan, A., Asrar, S., Raza, H., Das, R.K., Sahu, N.K., 2019. Synthesis of ZnO/Fe3O4/rGO nanocomposites and evaluation of antibacterial activities towards E. coli and S. aureus. IET Nanobiotechnol. 13, 682–687. https://doi.org/10.1049/iet-nbt.2018.5330.

Banerjee, S., Benjwal, P., Singh, M., Kar, K.K., 2018. Graphene oxide (rGO)-metal oxide (TiO2/Fe3O4) based nanocomposites for the removal of methylene blue. Appl. Surf. Sci. 439, 560–568. https://doi.org/10.1016/J.APSUSC.2018.01.085.

Behera, A., Kandi, D., Majhi, S.M., Martha, S., Parida, K., 2018. Facile synthesis of ZnFe2O4 photocatalysts for decolourization of organic dyes under solar irradiation. Beilstein J. Nanotechnol. 9, 436–446. https://doi.org/10.3762/bjnano.9.42.

Behera, A., Kandi, D., Mansingh, S., Martha, S., Parida, K., 2019. Facile synthesis of ZnFe2O4@RGO nanocomposites towards photocatalytic ciprofloxacin degradation and H2 energy production. J. Colloid Interface Sci. 556, 667–679. https://doi.org/10.1016/j.jcis.2019.08.109.

Biswal, B.M., Yusoff, Z., 2017. Application of nanotechnology in cancer treatment. Top. Mining Metall. Mater. Eng. 7, 269–311. https://doi.org/10.1007/978-3-319-29761-3_11.

Bray, F., Ferlay, J., Soerjomataram, I., Siegel, R.L., Torre, L.A., Jemal, A., 2018. Global cancer statistics 2018: GLOBOCAN estimates of incidence and mortality worldwide for 36 cancers in 185 countries. CA Cancer J. Clin. 68, 394–424. https://doi.org/10.3322/caac.21492.

Hidayah, N.M.S., Liu, W.W., Lai, C.W., Noriman, N.Z., Khe, C.S., Hashim, U., Lee, H.C., 2017. Comparison on graphite, graphene oxide and reduced graphene oxide: Synthesis and characterization. AIP Conf. Proc. 1892. https://doi.org/10.1063/1.5005764.

Hou, Y., Li, X., Zhao, Q., Chen, G., 2013. ZnFe2O4 multi-porous microbricks/graphene hybrid photocatalyst: Facile synthesis, improved activity and photocatalytic mechanism. Appl. Catal. B Environ. 142–143, 80–88. https://doi.org/10.1016/j.apcatb.2013.04.062.

Hou, L., Lian, L., Zhang, L., Pang, G., Yuan, C., Zhang, X., 2015. Self-sacrifice template fabrication of hierarchical mesoporous Bi-component-active ZnO/ZnFe2O4 sub-microcubes as superior anode towards high-performance lithium-ion battery. Adv. Funct. Mater. 25, 238–246. https://doi.org/10.1002/ADFM.201402827.

Kaur, J., Anand, K., Anand, K., Singh, R.C., 2018. WO3 nanolamellae/reduced graphene oxide nanocomposites for highly sensitive and selective acetone sensing. J. Mater. Sci. 53, 12894–12907. https://doi.org/10.1007/s10853-018-2558-z.

Khadgi, N., Li, Y., Upreti, A.R., Zhang, C., Zhang, W., Wang, Y., Wang, D., 2016. Enhanced photocatalytic degradation of 17α-ethinylestradiol exhibited by multifunctional ZnFe2O4-Ag/rGO nanocomposite under visible light. Photochem. Photobiol. 92, 238–246. https://doi.org/10.1111/php.12565.

Khadgi, N., Upreti, A.R., Li, Y., 2017. Simultaneous bacterial inactivation and degradation of an emerging pollutant under visible light by ZnFe2O4 co-modified with Ag and rGO. RSC Adv. 7, 27007–27016. https://doi.org/10.1039/c7ra01782k.

Kokila, N.R., Mahesh, B., Roopa, K.P., Prasad, B.D., Raj, K., Manjula, S.N., Mruthunjaya, K., Ramu, R., 2022. Thunbergia mysorensis mediated nano silver oxide for enhanced antibacterial, antioxidant, anticancer potential and in vitro hemolysis evaluation. J. Mol. Struct. 1255,. https://doi.org/10.1016/J.MOLSTRUC.2022.132455 132455.

Krishnan, S., Murugesan, S., Vasanthakumar, V., Priyadharsan, A., Alsawalha, M., Alomayri, T., Yuan, B., 2021. Facile green synthesis of ZnFe2O4/rGO nanohybrids and evaluation of its photocatalytic degradation of organic pollutant, photo antibacterial and cytotoxicity activities. Colloids Surfaces A Physicochem. Eng. Asp. 611,. https://doi.org/10.1016/j.colsurfa.2020.125835 125835.

Lai, W., Li, X., Li, B., Mei, J., Zhang, X., Guo, W., Peng, G., Li, H., Li, X., Yuan, J., 2021. MOF-derived ZnO/ZnFe2O4@RGO nanocomposites with high lithium storage performance. J. Solid State Electrochem. 25, 1175–1181. https://doi.org/10.1007/s10008-020-04891-w.

Lee, N., Yoo, D., Ling, D., Cho, M.H., Hyeon, T., Cheon, J., 2015. Iron oxide based nanoparticles for multimodal imaging and magnetoresponsive therapy. Chem. Rev. 115, 10637–10689. https://doi.org/10.1021/ACS.CHEMREV.5B00112/ASSET/IMAGES/LARGE/CR-2015-00112D_0007.JPEG.

Li, J., Zhou, D., 2020. Enhanced microwave absorption of reduced graphene oxide/Ni0.4Zn0.4Co0.2Fe2O4 composite at ultrathin thickness. J. Electron. Mater. 49, 1721–1727. https://doi.org/10.1007/s11664-019-07740-3.

Nadeem, N., Zahid, M., Tabasum, A., Mansha, A., Jilani, A., Bhatti, I.A., Bhatti, H.N., 2020. Degradation of reactive dye using heterogeneous photo-Fenton catalysts: ZnFe2O4 and GO-ZnFe2O4 composite. Mater. Res. Express 7. https://doi.org/10.1088/2053-1591/ab66ee.

Nguyen, V.Q., Baynosa, M.L., Nguyen, V.H., Tuma, D., Lee, Y.R., Shim, J.J., 2019. Solvent-driven morphology-controlled synthesis of highly efficient long-life ZnO/graphene nanocomposite photocatalysts for the practical degradation of organic wastewater under solar light. Appl. Surf. Sci. 486, 37–51. https://doi.org/10.1016/j.apsusc.2019.03.262.

Patterson, A., 1939. The Scherrer Formula for X-ray particle size determination. Phys. Rev. 56, 978–982. https://doi.org/10.1103/PhysRev.56.978.

Prasad, C., Murthy, P.K., Krishna, R.H.H., Rao, R.S., Suneetha, V., Venkateswarlu, P., 2017. Bio-inspired green synthesis of RGO/Fe3O4 magnetic nanoparticles using Murrayakoenigii leaves extract and its application for removal of Pb(II) from aqueous solution. J. Environ. Chem. Eng. 5, 4374–4380. https://doi.org/10.1016/J.JECE.2017.07.026.

Renukadevi, S., Pricilla Jeyakumari, A., 2020. Rational design of ZnFe2O4/g-C3N4 heterostructures composites for high efficient visible-light photocatalysis for degradation of aqueous organic pollutants. Inorg. Chem. Commun. 118,. https://doi.org/10.1016/j.inoche.2020.108047 108047.

Riaz, K., Nadeem, S., Chrouda, A., Iqbal, S., Mohyuddin, A., Hassan, S.U., Javed, M., BaQais, A., Tamam, N., Aroosh, K., Rauf, A., Abourehab, M.A.S., Jamil, M.I., Elkaeed, E.B., Alzhrani, R.M., Awwad, N.S., Ibrahium, H.A., 2022. Coupling of Se-ZnFe2O4 with rGO for spatially charged separated nanocomposites as an efficient photocatalyst for degradation of organic pollutants in natural sunlight. Colloids Surfaces A Physicochem. Eng. Asp. 649,. https://doi.org/10.1016/J.COLSURFA.2022.129332 129332.

Sarala, E., Madhukara Naik, M., Vinuth, M., Rami Reddy, Y.V., Sujatha, H.R., 2020. Green synthesis of Lawsonia inermis-mediated zinc ferrite nanoparticles for magnetic studies and anticancer activity against breast cancer (MCF-7) cell lines. J. Mater. Sci. Mater. Electron. 31, 8589–8596. https://doi.org/10.1007/s10854-020-03394-8.

Saranya, J., Saminathan, P., Ankireddy, S.R., Shaik, M.R., Khan, M., Khan, M., Shaik, B., 2023. Cerium oxide/graphene oxide hybrid: Synthesis, characterization, and evaluation of anticancer activity in a breast cancer cell line (MCF-7). Biomedicines 11. https://doi.org/10.3390/biomedicines11020531.

Shah, M.S.A.S., Zhang, K., Park, A.R., Kim, K.S., Park, N.G., Park, J.H., Yoo, P.J., 2013. Single-step solvothermal synthesis of mesoporous Ag-TiO2-reduced graphene oxide ternary composites with enhanced photocatalytic activity. Nanoscale 5, 5093–5101. https://doi.org/10.1039/C3NR00579H.

Shyamala, R., Gomathi Devi, L., 2020. Reduced graphene oxide/SnO2 nanocomposites for the photocatalytic degradation of rhodamine B: Preparation, characterization, photosensitization, vectorial charge transfer mechanism and identification of reaction intermediates. Chem. Phys. Lett. 748,. https://doi.org/10.1016/j.cplett.2020.137385 137385.

Somwanshi, S.B., Somvanshi, S.B., Kharat, P.B., 2020. Visible light driven photocatalytic activity of TiO2 nanoparticles prepared via gel-combustion process. J. Phys. Conf. Ser. 1644. https://doi.org/10.1088/1742-6596/1644/1/012042.

Sripriya, R.C., Samson, V.A.F., Anand, S., Madhavan, J., Raj, M.V.A., 2018. Comparative studies of structural, magnetic and photocatalytic degradation on 4-chlorophenol by ZnFe2O4 nanostructures prepared via cost effective combustion methods. J. Mater. Sci. Mater. Electron. 29, 14084–14092. https://doi.org/10.1007/s10854-018-9540-z.

Tabrez, S., Khan, A.U., Hoque, M., Suhail, M., Khan, M.I., Zughaibi, T.A., 2022a. Investigating the anticancer efficacy of biogenic synthesized MgONPs: An in vitro analysis. Front. Chem. 10, 1–14. https://doi.org/10.3389/fchem.2022.970193.

Tabrez, S., Khan, A.U., Hoque, M., Suhail, M., Khan, M.I., Zughaibi, T.A., 2022b. Biosynthesis of ZnO NPs from pumpkin seeds' extract and elucidation of its anticancer potential against breast cancer. Nanotechnol. Rev. 11, 2714–2725. https://doi.org/10.1515/ntrev-2022-0154.

Tabrez, S., Khan, A.U., Mirza, A.A., Suhail, M., Jabir, N.R., Zughaibi, T.A., Alam, M., 2022c. Biosynthesis of copper oxide nanoparticles and its therapeutic efficacy against colon cancer. Nanotechnol. Rev. 11, 1322–1331. https://doi.org/10.1515/ntrev-2022-0081.

Umekar, M.S., Bhusari, G.S., Potbhare, A.K., Mondal, A., Kapgate, B.P., Desimone, M.F., Chaudhary, R.G., 2021. Bioinspired reduced graphene oxide based nanohybrids for photocatalysis and antibacterial applications. Curr. Pharm. Biotechnol. 22, 1759–1781. https://doi.org/10.2174/1389201022666201231115826.

Wang, E.R., Shih, K.Y., 2021. Facile microwave hydrothermal synthesis of znfe2o4/rgo nanocomposites and their ultra-fast adsorption of methylene blue dye. Materials (Basel). 14. https://doi.org/10.3390/ma14185394.

Wu, S., Wang, P., Cai, Y., Liang, D., Ye, Y., Tian, Z., Liu, J., Liang, C., 2015. Reduced graphene oxide anchored magnetic ZnFe2O4 nanoparticles with enhanced visible-light photocatalytic activity. RSC Adv. 5, 9069–9074. https://doi.org/10.1039/c4ra14587a.

Xie, T., Xu, L., Liu, C., Wang, Y., 2013. Magnetic composite ZnFe 2 O 4 /SrFe 12 O 19: Preparation, characterization, and photocatalytic activity under visible light. Appl. Surf. Sci. 273, 684–691. https://doi.org/10.1016/j.apsusc.2013.02.113.

Yuan, C., Cao, H., Zhu, S., Hua, H., Hou, L., 2015. Core–shell ZnO/ZnFe2O4@C mesoporous nanospheres with enhanced lithium storage properties towards high-performance Li-ion batteries. J. Mater. Chem. A 3, 20389–20398. https://doi.org/10.1039/C5TA05984D.

Zamani, A., Sadjadi, M.S., Mahjoub, A., Yousefi, M., Farhadyar, N., 2020. Synthesis, characterization and investigation of photocatalytic activity of ZnFe2O4@MnO–GO and ZnFe2O4@MnO–rGO nanocomposites for degradation of dye Congo red from wastewater under visible light irradiation. Res. Chem. Intermed. 46, 33–61. https://doi.org/10.1007/s11164-019-03934-w.

Zhang, R., Huang, X., Zhong, B., Xia, L., Wen, G., Zhou, Y., 2016. Enhanced microwave absorption properties of ferroferric oxide/graphene composites with a controllable microstructure. RSC Adv. 6, 16952–16962. https://doi.org/10.1039/C5RA22254K.

Zhao, Y., Ikram, M., Wang, J., Liu, Z., Du, L., Zhou, J., Kan, K., Zhang, W., Li, L., Shi, K., Zhao, Y., Ikram, M., Wang, J., Liu, Z., Du, L., Zhou, J., Kan, K., Zhang, W., Li, L., Shi, K., 2017. Ultrafast NH3 sensing properties of WO3@CoWO4 heterojunction nanofibres at room temperature. Aust. J. Chem. 71, 87–94. https://doi.org/10.1071/CH17354.

Zughaibi, T.A., Mirza, A.A., Suhail, M., Jabir, N.R., Zaidi, S.K., Wasi, S., Zawawi, A., Tabrez, S., 2022. Evaluation of anticancer potential of biogenic copper oxide nanoparticles (CuO NPs) against breast cancer. J. Nanomater. 2022. https://doi.org/10.1155/2022/5326355.